

Supramolecular Assembly of U(IV) Clusters and Superatoms with Unconventional Counterions

Ian Colliard, Gregory Morrison, Hans-Conrad zur Loya, and May Nyman*



Cite This: <https://dx.doi.org/10.1021/jacs.0c03041>



Read Online

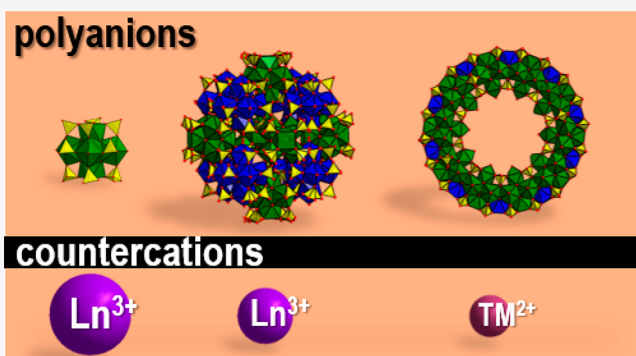
ACCESS |

Metrics & More

Article Recommendations

Supporting Information

ABSTRACT: Superatoms are nanometer-sized molecules or particles that form ordered lattices, mimicking their atomic counterparts. Hierarchical assembly of superatoms gives rise to emergent properties in lattices of quantum dots, p-block clusters, and fullerenes. Here, we introduce a family of uranium-oxysulfate cluster anions whose hierarchical assembly in water is controlled by two parameters: acidity and the lanthanide or transition-metal counterion. In acid, larger Ln^{III} (Ln = La–Ho) link hexamer (U₆) oxoclusters into body-centered cubic frameworks, while smaller Ln^{III} (Ln = Er–Lu and Y) promote linking of 14 U₆ clusters into hollow superclusters (U₈₄ superatoms). U₈₄ assembles into superlattices including cubic-closest packed, body-centered cubic, and interpenetrating networks, bridged by interstitial counterions and U₆ clusters. Divalent transition metals (TM = Mn^{II} and Zn^{II}) charge-balance and promote the fusion of 10 U₆ and 10 U monomers into a wheel-shaped cluster (U₇₀). Dissolution of U₇₀ in organic media reveals (by small-angle X-ray scattering) that differing supramolecular assemblies are accessed, controlled by TM^{II}-linking of U₇₀ clusters. Magnetic measurements of these assemblies reveal Curie–Weiss behavior at high temperatures, without pairing of the 5f²-electrons down to 2 K.



INTRODUCTION

Molecular fractals and supramolecular assemblies are studied to understand the underlying rules of complex assemblies and to access materials and molecules with multiscale properties. Molecular fractals are strategically synthesized via organic and coordination chemistry in metallocycles,^{1,2} dendrimers,^{3,4} and proteins.⁵ Inorganic materials that exhibit multiscale structure replication via supramolecular assembly are rare. Rather, these phenomena have been observed at a nonmolecular level in the self-assembly of nanomaterials including CdSe nanorods,⁶ and silver nanosheets.⁷ Bimodal, monodisperse nanoparticles with organic capping groups and C₆₀-fullerenes behave as “superatoms”,⁸ assembling into lattices that resemble binary compound structure types.⁹ In addition, semiconducting p-block Zintl-cluster anions¹⁰ (i.e., As₇³⁻, Al₁₃¹⁻) can be assembled through counterion linking into different structures exhibiting unique electronic properties.^{11,12}

Supramolecular assembly of polynuclear metal-oxo clusters has led to revolutionary discoveries in materials chemistry, including synthetic zeolites and metal–organic frameworks (MOFs). The UiO-66¹³ MOF, widely exploited for its stability and adaptability to different applications, is built of hexanuclear, Zr₆ oxo clusters, isostructural with U₆ (described later). A cluster building block of zeolites consists of eight corner-linked (Al,Si)O₄ tetrahedra, and these clusters have been both isolated in the molecular form^{14,15} and shown to self-assemble in solution¹⁶ prior to crystallization of zeolites. In

between isolated polynuclear cluster molecules and infinite lattices built from such clusters is any number of hypothetical entities; i.e., assemblies of clusters or prenucleation “clusters of clusters”. One example of these, metal organic polyhedra, MOPs, were designed and developed almost in parallel with MOFs, consisting of small cages joined by ditopic linkers.¹⁷ In polyoxometalate chemistry, there are examples of “super-clusters” that are composed of smaller identifiable cluster units. These include (1) the giant molybdate wheels and capsules pioneered by Muller that contain numerous molybdate cluster building units plus heterometals,¹⁸ (2) tetramer rings of P₂W₁₂ with endohedral and linking metals,^{19,20} (3) Nb₂₄ clusters linked by heterometals into larger assemblies,^{21–23} and (4) a supertetrahedral assembly of uranyl peroxide capsules,²⁴ an actinyl POM pioneered by Burns.²⁵

Assembly of actinide clusters into materials is far less prolific. One of the most common cluster motifs is the aforementioned hexamer [M^{IV}₆(OH)₄(O)₄]¹²⁺ (M = An including Th, U, Np, Pu, and also Zr/Hf) stabilized by various carboxylate groups,

Received: March 19, 2020

Published: April 22, 2020

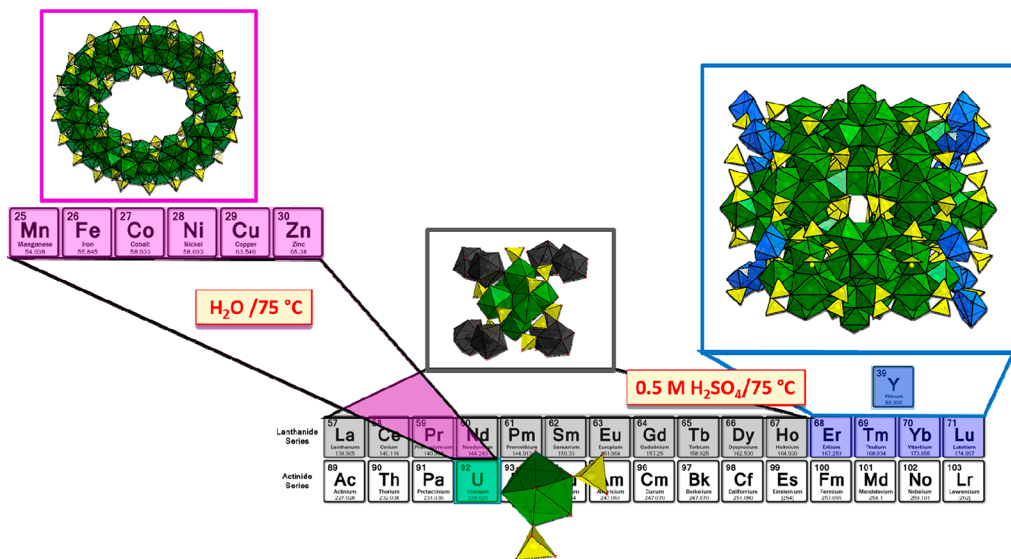


Figure 1. Summary of U^{IV} -sulfate TM/Ln phases. Schematic summarizes the reaction of $\text{U}(\text{SO}_4)_2$ with (1) divalent transition metals charge-balancing U_{70} (top left), (2) large Ln^{III} building U_6 -frameworks (middle), and (3) small Ln^{III} charge-balancing U_{84} (right). Note: structures presented here are with countercations $\text{Ln} = \text{La}, \text{Er}, \text{Lu}$, and Y ; and $\text{TM} = \text{Mn}$ and Zn . Other analogues (including $\text{TM} = \text{Fe}-\text{Ni}$ and $\text{Ln} = \text{Ce}-\text{Ho}$, except Pm) will be presented in subsequent publications. Green and yellow polyhedra are respectively U^{IV} -oxo and SO_4^{2-} , black polyhedra are large Ln^{III} -oxo, and blue polyhedra are small Ln^{III} -oxo. Details of these structures are in subsequent text and figures.

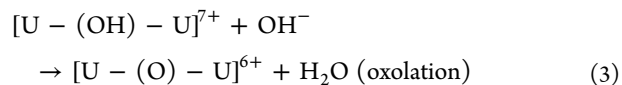
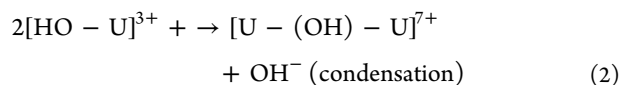
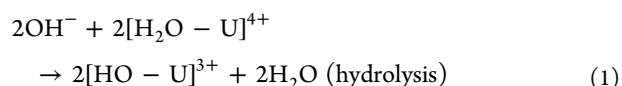
triflates, selenate, and sulfate.^{26–31} Researchers have synthesized MOFs and inorganic frameworks (including interpenetrating frameworks²⁹) featuring linked Th_6 , U_6 ,^{34,35} and Np_6 ³⁶ nodes. The An_6 cluster is also an exact building block of AnO_2 . Recently, clusters ranging in nuclearity from An_{10} – An_{38} have been isolated that are larger fragments of AnO_2 ,^{37–43} elucidating understanding of colloidal actinide transport in the environment.⁴⁴ U^{IV} -sulfate speciation^{45,46} (with heterometals) is of special relevance to biogeochemical activity in uranium ore deposits, mining sites, and the contaminated subsurface. Sulfur oxidizing bacteria immobilizes uranium as discrete UO_2 nanoparticles⁴⁷ (~ 2 nm) that are similar in dimensions to the clusters described herein.

Here, we introduce a family of U^{IV} -oxo-sulfate cluster superlattices. Polyoxoanion clusters assemble with lanthanide (Ln^{III}) and transition metal (TM^{II}) countercations, where the size and geometry of the polyanion (containing 6, 70, or 84 U^{IV} centers, respectively U_6 , U_{70} , and U_{84}) can be rationalized by acidity of the reaction media and size and bonding-covalency of the Ln or TM countercation (summarized in Figure 1). U_{84} , is a “cluster-of-clusters” superatom, highlighted in three different superlattices with three generations of structural similarity, linked by Ln^{III} , U^{IV} monomers, and U_6 . U_{70} is a wheel structure unlike any prior-reported U^{IV} cluster that is charge-balanced and assembled with TM^{II} countercations (Mn, Zn reported here; others will be subsequently reported) in low-acidity media. In three different lattices, these also display complex supramolecular assembly, including sandwiching U_6 units. Different bonding behavior of Zn^{2+} and Mn^{2+} to U_{70} in the solid-state are preserved in solution, further underlining the importance of these counterions on assembly processes. Transition metal toroid or wheel clusters have been previously discovered that include a Zr_{25} ring polycation,⁴⁸ an organically ligated neutral $\text{Mn}^{\text{IV}}_{70}$ ring,⁴⁹ and an anionic phosphate/acetate ligated Pd_{84} ring.⁵⁰ However, this is the first example of an An^{IV} -oxo cluster that does not build symmetrically on a central An_6 core, similar to

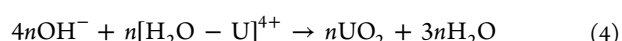
AnO_2 .^{40,41,43,51} U_{70} and U_{84} are the largest tetravalent actinide (or $\text{Zr}/\text{Hf}^{\text{IV}}$) molecular clusters observed to date, strategically isolated with nonconventional, high-valence countercations.⁵²

RESULTS AND DISCUSSION

All tetravalent metals, including U^{IV} , exhibit strong hydrolysis behavior. Upon dissolution in water, the highly charged cations bind water and deprotonate, leading to formation of oligomers, even in aqueous acid.⁵³ The fundamental hydrolysis, condensation, and oxolation reactions describing this process are



In initial syntheses, we dissolved rare earth oxides in the acidic solutions with the hypothesis of driving this reaction by locally generating hydroxide, i.e. $\text{La}_2\text{O}_3 + 3\text{H}_2\text{O} \rightarrow 2\text{La}^{3+} + 6\text{OH}^-$. After initial discovery of the crystalline forms, combinations of Ln salts and oxides were used to maximize purity and yield. This *in situ* partial neutralization proved effective prior for isolation of an aluminum-octamer polyoxocation.⁵⁴ *In situ* production of hydroxide in this manner is more controlled than adding a strong base, which temporarily creates local high concentrations of hydroxide. UO_2 is the thermodynamic product of hydrolysis–condensation–oxolation reactions, generally described as



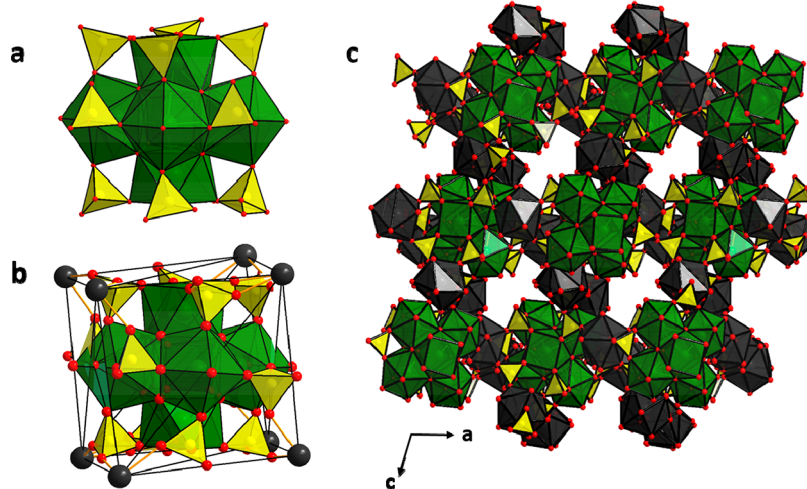


Figure 2. Ln-U_6 frameworks. (a) Polyhedral representation of $[\text{U}_6(\text{OH})_4(\text{O})_4(\text{SO}_4)_{12}]^{12-}$: U^{IV} polyhedra are green, sulfate polyhedra are yellow, O atoms are red spheres. (b) Highlighting the linkage between La^{III} (black spheres) and U_6 . (c) Polyhedral representation of La-U_6 framework, showing void channels along the b -axis.

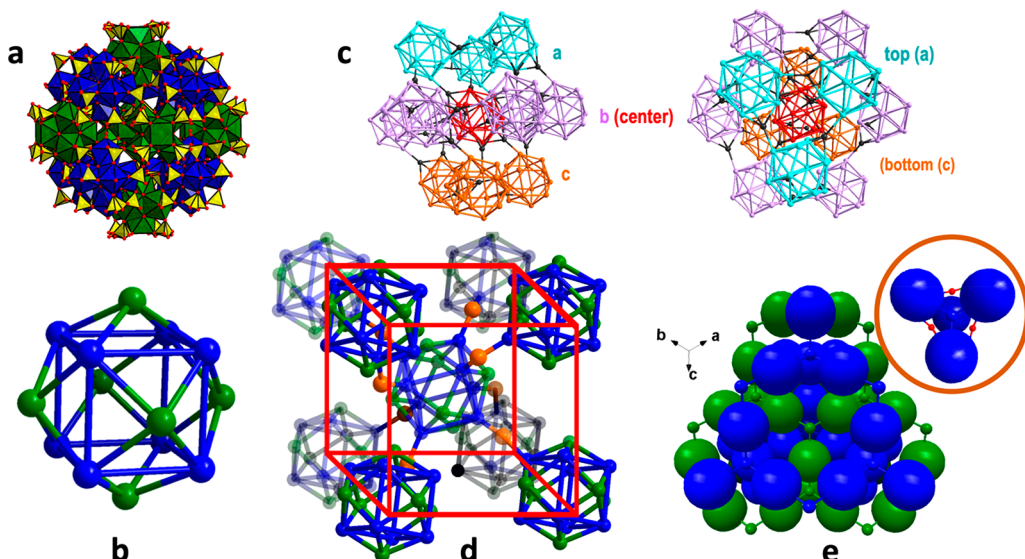


Figure 3. U_{84} and its superlattices. (a) Polyhedral representation of U_{84} . U_{6c} (corner) are blue, U_{6f} (face) are green, sulfate is yellow. (b) Simplified representation of U_{84} replacing the U_6 units with green (U_{6f}) and blue (U_{6c}) spheres. (c) View of Y-U_{84} highlighting the cubic closest packing of the U_{84} superatoms, linked by Y monomers (black spheres). (d) View of LuU-U_{84} , highlighting the body-centered cubic arrangement of U_{84} , bridged by U^{IV} monomers (orange). (e) Simplified representation of $\text{ErU}_6-(\text{U}_{84})_2$, highlighting the two diamondoid interpenetrating networks (respectively green and blue). Large spheres are U_{84} , linked by U_6 (small spheres). Each tetrahedral network is also bridged by partially occupied Er^{III} (inset, red spheres linking blue network).

Additionally, the strongly coordinating sulfate ions in these reactions compete with the hydrolysis reactions, allowing assembly of cluster-based framework materials.

U^{IV} -Lanthanide Assemblies. Combining larger lanthanides, such as La^{III} , leads to the assembly of frameworks consisting of U_6 that are bridged by the heterometal center. We have crystallized different arrangements of these from $\text{Ln} = \text{La} - \text{Ho}$. We describe the prototype La-U_6 here as an example; others will be described in subsequent publications. La-U_6 , formulated $\text{La}_4\text{U}_6(\text{OH})_4(\text{O})_4(\text{SO}_4)_{12}(\text{H}_2\text{O})_{20}$, crystallizes in the monoclinic space group $P2_1/a$ (Table SI-1). The U^{IV} hexamer is the typical core $[\text{U}_6(\text{OH})_4(\text{O})_4]^{12+}$, exhibiting oxo-hydroxo disorder (Figure SI-1). The first U_6 -sulfate was reported in 1953⁵⁵ and then not again until very recently.³⁰ The core U_6 -sulfate anion (Figure 2a) is a recurring moiety

throughout the structures described here. The charge-balancing La^{III} bridge two hexamers via sulfate groups. Each U_6 -hexamer can be described as a distorted cube, with its six polyhedra occupying the six cube faces and eight La located on the cube corners (Figure 2b). A framework arises from the “corner-to-corner” linkages of bridging La monomers. Due to the 3d-checkerboard linkage, La-U_6 exhibits large voids that contain disordered lattice waters (Figure 2c, Table SI-9).

With the smaller Ln^{III} (Er-Lu and Y) as counterions, a second-generation assembly of U_6 is observed. Fourteen sulfate-bridged U_6 clusters assemble into a hollow sphere; a U_6 occupying the six faces and the eight corners of a cube (Figure 3a and b), totaling 84 U^{IV}^- centers, comprising a U_{84} superatom. The U_6 of the corner positions, (blue , U_{6c}) have 12 bridging sulfates, while the face U_6 (green , U_{6f}) possess 16

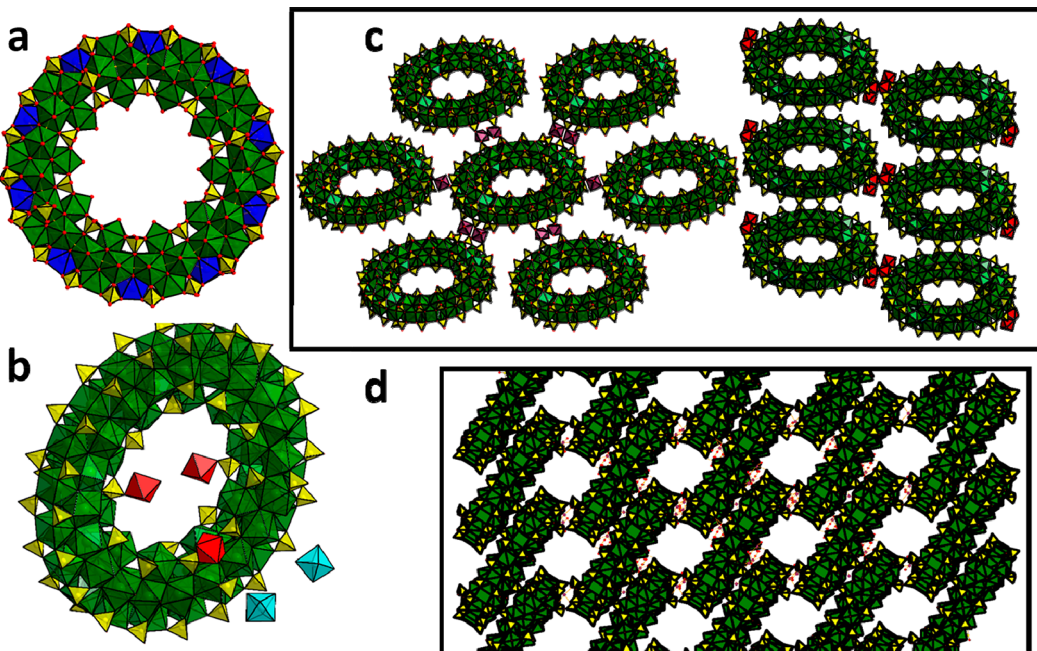


Figure 4. TM^{II}-U₇₀. (a) Polyhedral representation of U₇₀ highlighting the monomer and hexamer units. U^{IV} monomer in blue and U₆ unit in green, sulfur in yellow, oxygen atoms are red spheres. (b) Representation of Zn-U₇₀, emphasizing the coordination environments of Zn. The red octahedra are Zn, linked to U₇₀ via corner-sharing with sulfate. These sit just above the central cavity. The turquoise octahedra are Zn(H₂O)₆ that are located between U₇₀ rings, unassociated. (c) Mn-U₇₀ (left) and Zn-U₇₀ (right) highlighting the difference in cluster linking via Mn-octahedra (purple) and Zn-polyhedra (red). (d) View of Mn-U₇₀ lattice stacking arrangement (approximately perpendicular to the viewing direction in c).

sulfates. Each U_{6f} is linked to four U_{6c} along the diagonals of the U₈₄-cube face. Likewise, each U_{6c} is linked to three U_{6f}. Each U_{6f}-U_{6c} linkage is through three bridging sulfates, reinforcing the rigid U₈₄.

To understand this structure switch with decreasing lanthanide radius, we first consider reaction conditions, namely pH and metal concentration (which influences pH). Uranium concentration is 0.46 molar for each reaction, while Ln:U ratios include ~0.5 (La and Er), ~1.0 (Lu), and ~4.0 (Y). These wide-ranging concentrations were empirically tailored for each experiment to optimize purity and yield of the crystalline product. The starting and ending pH of each reaction is 1.50 and 2.25, respectively, suggesting there is little pH influence of the lanthanides on in the 0.5 molar H₂SO₄, 0.46 molar U^{IV} reaction medium. The postreaction pH increase is commensurate with decreased concentration of all species in solution upon crystallization of the product. Thus, metal concentration and pH likely do not strongly influence the assembly of U₆-frameworks vs U₈₄.

Simple ion size of Ln^{III} is an additional factor to consider. The U₈₄-forming metals (Y, Er, Lu) have ionic volumes ranging from 4.2 to 4.7 Å³, while La^{III} is 6.7 Å³. Perhaps the smaller ions are not large enough to span two or more coordinating U₆ to build a framework. We can also rationalize this structure switch from lanthanide-linked U₆ frameworks to U₈₄ assemblies that occlude the Ln^{III} counterions with a description of Ln-bonding that includes covalent contribution from the 5d orbitals. Loble and coworkers⁵⁶ recently developed a detailed model of Ln³⁺-bonding trends in rare earth chlorides from chlorine X-ray absorption spectroscopy and density functional theory calculations. They noted mixing between the Cl 3p- and Ln 5d-orbitals, which decreases across the series. Contraction of these orbitals across the series diminishes the ability of Ln to participate in covalent network

assembly. Relating these prior studies to our results, we propose that La^{III} disrupts linkage between U₆ units and forms frameworks, while Lu^{III} behaves more as a classic counterion in the superlattice, *vide infra*. Three structures displaying differentiating third-generation assembly of U₈₄ superatoms are described below.

Y-U₈₄, formulated Y₁₆[U₆(OH)₄(O)₄]₁₄(SO₄)₁₀₈(H₂O)_{126.5}, crystallizes in the tetragonal P4/m space group (volume = 39 627 Å³, Table SI-2). Each U₈₄ is surrounded by 12 U₈₄ units, resembling cubic closest packing of equal-sized spheres, defining the third-generation of supramolecular assembly. U₈₄ are bridged by Y^{III} via the eight U_{6c} corners (Figure 3c) and four of the U_{6f} faces. Y^{III} monomers (7–8 coordinate) decorate and bridge the U₈₄ clusters through sulfate bridges.

For mu 1 a t e d U₄Lu₁₂(U₆(OH)₄(O)₄)₁₄(SO₄)₁₁₀(H₂O)₈₀ crystallizes in the trigonal R3c space group (volume = 137 813 Å³, Table SI-4). LuU-U₈₄ can be described as a body centered cubic arrangement of U₈₄ (Figure 3d), linked by U^{IV} monomers that are bridged by corner-sharing sulfates. Partially occupied Lu^{III} also decorates and bridges U₈₄ via the sulfates, but the main connectivity is defined by U^{IV} monomers. Notable is the multiscale replication of patterns: this linking of U₈₄ joined by monomers at the eight-corner U_{6c} is similar to the first structure described (La-U₆), where U₆ are linked by corners via La^{III} monomers.

ErU₆-(U₈₄)₂, formulated U₆(OH)₄(O)₄(H₂O)₁₂-[Er₁₆(U₆(OH)₄(O)₄)₁₄(SO₄)₁₁₁(H₂O)₁₃₀]₂ (Table SI-3), crystallizes in the cubic space group Pn3 (volume = 84 891 Å³). In ErU₆-(U₈₄)₂, rotationally disordered U₆ (U_{6tet} for this discussion, disorder detailed in the Supporting Information) occupies half the tetrahedral voids of closest packed U₈₄ and links to the U_{6c} via sulfate bridges. There are two interpenetrating tetrahedral ErU₆-(U₈₄)₂ networks, shown in green

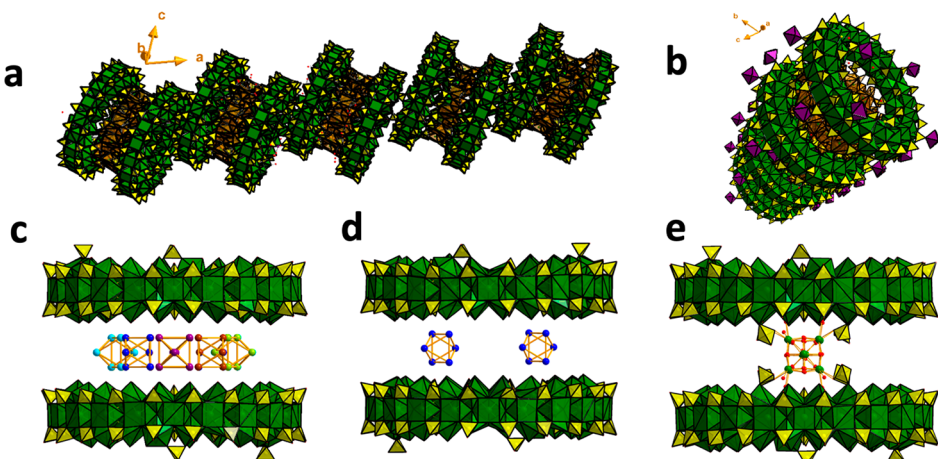


Figure 5. U₇₀-U₆-U₇₀ sandwich. (a) View of the U₇₀-U₆-U₇₀ sandwich stacking in Mn-(U₆U₇₀)₂. Bright green polyhedra are U^{IV}-oxo of U₇₀, brown polyhedra are the disordered hexamers, yellow polyhedra are sulfate. (b) Approximately perpendicular view of the U₇₀-U₆-U₇₀ sandwich stacks, showing linkage of the Mn-octahedra (purple), corner-sharing with sulfate. (c) View of the five settings of the U₆ cluster inside the sandwich. Only the uranium is shown in turquoise, blue, purple, brick, and chartreuse (left to right). (d) Illustration of the 1/5th occupancy of U₆ as pairs on opposite sides of the wheel (blue). (e) Highlighting connectivity of U₆ via four sulfate bridges to the U₇₀ rings.

and blue in Figure 3e. The U₈₄ units are also connected by Er^{III}-monomer-sulfate-U_{6f} linkages (Figure 3e, inset).

U^{IV} Transition Metal Assemblies. The addition of first row divalent transition metals (TM^{II}, in the form of acetate salts) to the aqueous uranium sulfate salt leads to a different cluster assembly. While 0.5 molar sulfuric acid was optimal to keep the Ln^{III}-U^{IV} reactants dissolved, the first row TM^{II} can dissolve in water only. The lack of coordinating sulfate and lower acidity is conducive to more extensive hydrolysis. However, instead of yielding the end-product UO₂, TM^{II} stabilizes and charge-balances a U₇₀ ring with the core formula [U₇₀(OH)₃₆(O)₆₄(SO₄)₆₀]⁴⁻ (Figures 1 and 4). Mn^{II} and Zn^{II} analogues are introduced here, and others will be described in subsequent publications.

The U₇₀ ring features 70 U^{IV} centers fused by oxo/hydroxo ligands. It can be viewed as ten alternating U₆ and U^{IV} monomers (Figure 4a). The U₆ subunit has the typical core formula of [U₆(OH)₄(O)₄]¹²⁺. However, instead of 12 bridging sulfates, it possesses only 8: 4 bridging the outer ring and 4 bridging the inner ring. The outer sulfates link to the U^{IV} monomer, while the inner sulfates bridge to neighboring hexamers, creating curvature. The entirety of the ring structure exhibits oxo/hydroxo disorder, determined by bond valence sum calculations (Table SI-11). All the uranium centers are 8-coordinate with the exception of the innermost uranium of the U₆ units. These are 9-coordinate, due to an additional bound water. Additional terminally bound sulfates link the rings in an offset “face-to-face” manner in the different assemblages (Figure 4d).

Mn-U₇₀, formulated Mn₆U₇₀(OH)₃₆(O)₆₄(SO₄)₆₄(H₂O)₄₄, crystallizes in the triclinic P1 space group (volume = 16 367 Å³, Table SI-5). The U₇₀ rings are stacked offset and face-to-face, approximately along the *a*-direction. They are linked together by both bridging sulfates and Mn^{II}-octahedra. The Mn^{II}-octahedra also join the stacks together nearly perpendicular to the stacking direction (Figure 4d), leading to a fully connected framework (Figure 4c) with large pores (Table SI-9).

TBACl (tetrabutylammonium chloride, see Supporting Information for synthesis details) was included in the Mn-U₇₀ synthesis medium, which can mediate the formation and supramolecular assembly of the U₇₀ rings by changing the ionic

strength of the system. Nonbonding “innocent” cations such as TBA⁺ will shield interactions between U^{IV} species during assembly processes. We expect U₆, U-sulfate monomers, and U₇₀ to all be present in the reaction solution, which can interact and potentially link together. In the above-described assembly of Mn-U₇₀, we presume TBA⁺ (and to a lesser extent Cl⁻) partially shield these interactions. In a similar synthesis, without added TBACl (see Supporting Information for details), we obtain a U₇₀-(U₆)₂-U₇₀ sandwich, Mn-(U₆U₇₀)₂, formulated Mn₄(H₂O)₁₆[{(U₆(OH)₄(O)₄)(H₂O)₉]- (U₇₀(OH)₃₄(O)₆₆(SO₄)₆₅(H₂O)₆₁]₂. Mn-(U₆U₇₀)₂ crystallizes in the triclinic P1 space group (volume = 37 244 Å³, Table SI-6) The U₇₀-(U₆)₂-U₇₀ sandwich contains two U₆ clusters on opposite sides and between two U₇₀ rings. Four sulfates of U₆ bridge to the ring on the outside, while the inner association is via hydrogen-bonding between U₆ and U₇₀ (Figure 5c). The U₆ pairs are disordered over five positions, consistent with the tenfold symmetry of the U₇₀ ring (Figure 5c). Details describing this disorder are included in the Supporting Information. Chains of the [U₇₀-(U₆)₂-U₇₀]_n run approximately along the *a*-axis (Figure 5a and b), with similar offset of stacking found in Mn-U₇₀. In addition, the charge-balancing Mn^{II} monomers link the chains of rings in the opposite direction (approximately in the BC-plane) via bridging sulfates of neighboring U₇₀.

Zn-U₇₀ was also obtained with the TBACl “mineralizer”. It is fully formulated (Zn(H₂O)₆)_{3.5}Zn_{2.5}U₇₀(OH)₃₆(O)₆₄(SO₄)₆₄(H₂O)_{54.5} and crystallizes in the triclinic P1 space group (volume = 14 801 Å³, Table SI-7). Zn-U₇₀ presents an arrangement in the lattice similar to that of Mn-U₇₀ (Figure 4c). However, an important distinction is the lack of any linking of U₇₀ between or within the stacks via Zn²⁺. Of the four Zn-sites, two are fully coordinated to water, and the other two bind inside the U₇₀ ring (Figure 4b). The 3d¹⁰ electron configuration of Zn^{II} minimizes covalent linkage to the sulfate ligands, as recently described in X-ray absorption studies.⁵⁷ In this prior study, pre-edge features in sulfur K-edge X-ray absorption spectra were observed for sulfate complexes of Co(II), Ni(II), and Cu(II) but not Zn(II). The authors attributed this to ligand (sulfate) contributions to the 3d LUMO of the divalent transition metal, which is not possible

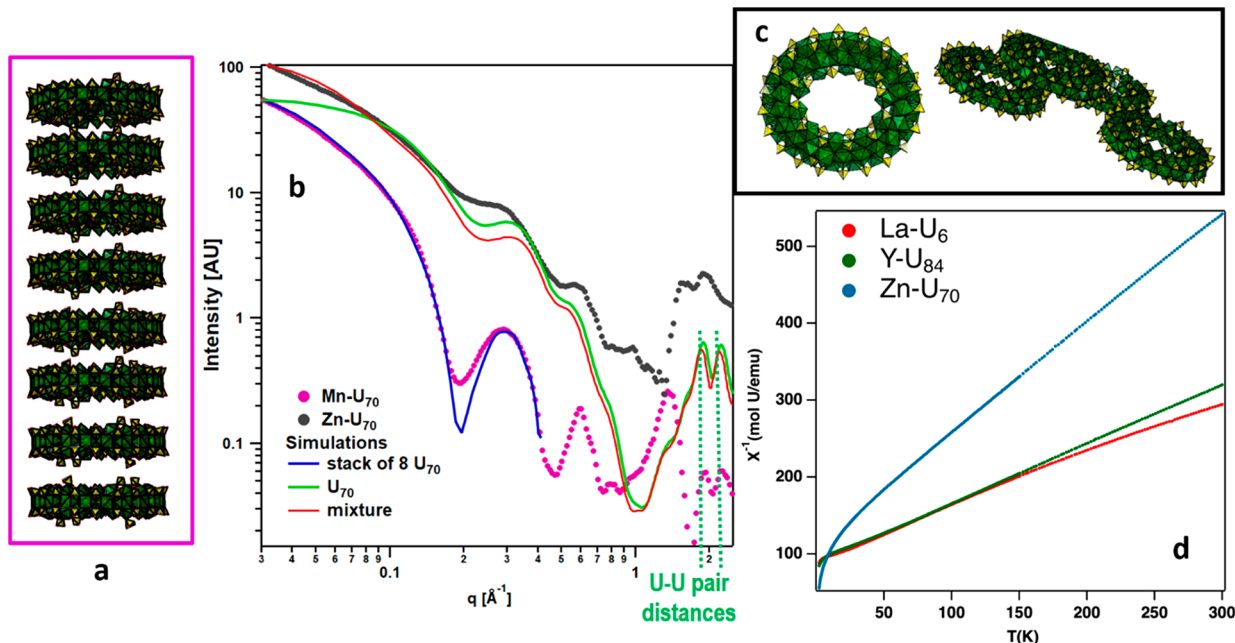


Figure 6. X-ray scattering of dissolved U₇₀ and magnetic susceptibility. (a) Hypothetical stack of eight U₇₀; its simulated scattering data matches those of Mn-U₇₀ (simulated scattering shown in blue in panel b). (b) Experimental scattering data for Mn-U₇₀ (pink) and Zn-U₇₀ (black) in 1:3 THF:butylamine solvent mixture. (c) Isolated U₇₀ (simulated scattering data in green), plus aggregate of four U₇₀, $[\text{U}_{70}]_4$. Simulated scattering data for 90% U₇₀ and 10% $[\text{U}_{70}]_4$ is shown in red. This approximate mixture is proposed for dissolved Zn-U₇₀, as determined by size distribution analysis of experimental scattering data (see Figure SI-10). (d) Magnetic susceptibilities of La-U₆, Y-U₈₄, Zn-U₇₀ measured under zfc conditions and an applied field of 1000 Oe.

for closed-shell Zn^{II}. This differing degree of TM^{II}-U₇₀ connectivity, along with the U₆ → U₈₄ structure switch in response to Ln^{III} bonding character, highlights the importance of multivalent counterions in isolating these unique U^{IV}-sulfate assemblies.

Small Angle X-ray Scattering. The extensive U₇₀-Mn^{II}-U₇₀ and minimal U₇₀-Zn^{II}-U₇₀ connectivity observed in the solid-state compounds was also evidenced upon dissolution. Despite the entirely inorganic nature of the U₇₀ ring, its aqueous synthesis, and its interconnectivity in various frameworks, it can be dissolved intact in organic media (1:3 THF:butylamine), perhaps because of the extremely low charge density of the cluster (~4 per 70 metal centers). The small-angle scattering intensity for dissolved Zn-U₇₀ and Mn-U₇₀ is strong due to their large size and the strong scattering power of uranium (Figure 6b). The average-size species for dissolved Mn-U₇₀ is considerably larger than that for Zn-U₇₀, indicated by the Guinier region shift to lower q for the former. The Guinier region is the steep negative-slope at low q ($q < 0.15 \text{ \AA}^{-1}$ for Mn-U₇₀; $q < 0.20 \text{ \AA}^{-1}$ for Zn-U₇₀). The Mn-U₇₀ curve is ideally fit with a core-shell cylindrical model (Table SI-12, Figure SI-9) that matches well with simulated scattering data for a hypothetical stack of eight U₇₀ rings (Figure 6a). We can confidently say this is the main aggregate present in this solution, and that Mn^{II} links the clusters in addition to the sulfate. Comparing the Zn-U₇₀ scattering to the simulated U₇₀ monomer scattering shows a good match between $\sim q = 0.1 - 0.8 \text{ \AA}^{-1}$. Moreover, the two plateaus between $q \sim 0.2$ and 0.8 \AA^{-1} are observed in both the simulated and experimental scattering, strong evidence that the Zn-U₇₀ solution is dominated by isolated clusters. However, the upward slope at $q > 0.1 \text{ \AA}^{-1}$ indicates formation of aggregates. Analysis of the size distribution suggests the majority of the dissolved aggregates are around 35 Å (U₇₀ monomers) in diameter,

with a larger population of ~80 Å (ratio of U₇₀:aggregates ~9:1, Figure 6c). Based on inspecting and simulating SAXS data for various U₇₀ aggregates observed in the crystal structures, we propose the modest amount linking promoted by Zn is via staggered stacking rather than perfectly eclipsed, as observed for dissolved Mn-U₇₀. The oscillations and other features at high q (i.e., the peaks around 2 \AA^{-1}) that give information on shape and atom–atom distances are also present in both the experimental and simulated scattering curves. It is interesting that the eclipsed stacking that is so prevalent in the Mn-U₇₀ solution has not been observed in solid-state structures presented here, nor in other structures we have obtained that will be reported shortly. Perhaps the butylamine stabilizes the cylindrical stacks via inverse micelle formation. This suggests other supramolecular assemblies may be accessible via dissolution of U₇₀ in organic media containing various TM linkers and surfactants. Use of capping amphiphiles is a strategy used prior to create superlattices of nanoparticles.^{58,59}

Magnetic Measurements. While magnetic ordering and frustration has been discovered in polynuclear TM, Ln, and TM-Ln single-molecule magnets,⁶⁰ similar studies of An-TM/Ln have been less explored, partly due to a paucity of synthesized species. In fact, only one magnetic measurement of U^{IV}-oxo clusters (U₆)⁶¹ and two of U₃₈^{39,51} have been executed. Similar to U^{IV} oxides, U₆ and U₃₈ exhibit transition of the 5f² electrons from unpaired to paired with cooling. Typically, high coordination U^{IV} compounds (CN = 8) exhibit Curie–Weiss behavior,⁶² whereas lower coordination numbers (CN = 6) lead to non-Curie-like behavior due to strong crystalline electric field effects.⁶³ Recently, a Mn-U^{IV} fluoride was described with magnetic coupling between the 3d and 5f electrons,⁶⁴ piquing interest in magnetic properties of U^{IV}-TM/Ln oxo clusters and oxides.

Figure 6d shows the magnetic susceptibility of La-U₆, Y-U₈₄, and Zn-U₇₀, and these magnetic data plus those for Mn-U₇₀ are summarized in Table 1. In the first three compounds, U^{IV} is

Table 1. Magnetic Properties of Reported Phases^a

	θ (K)	μ_{eff} (μ_B/FU)	μ_{calc} (μ_B/FU)	μ_{eff} (μ_B/U)	μ_{calc} (μ_B/U)
La-U ₆	-140(3)			3.58(3)	3.58
Y-U ₈₄	-112(3)			3.21(3)	3.58
Zn-U ₇₀	-79(2)			2.36(3)	3.58
Mn-U ₇₀	-28.2(6)	27.93(9)	33.28	2.85(3) ^b	3.58

^aAll data fit to the Curie–Weiss law from 50–300 K. ^bCalculated assuming an observed moment of 5.92 μ_B/Mn .

the only magnetic ion, allowing for direct observation of the U^{IV} magnetic behavior. All three compounds exhibit Curie–Weiss behavior at high temperatures, without pairing of the 5f² electrons down to 2 K. Fitting the 50–300 K data to the Curie–Weiss law yields effective moments of 3.58(3) μ_B/U (La-U₆), 3.19(3) μ_B/U (Y-U₈₄), and 2.36(3) (Zn-U₇₀). Because of the non-Curie like behavior of many U^{IV} compounds, the uranium moment is often estimated as 2.827(χT)^{1/2} at 300 K, yielding moments reported in Table 1. The observed moment for La-U₆ extracted from the Curie–Weiss fit is in excellent agreement with the calculated moment of 3.58 μ_B/U for U^{IV}, and the others are within the reported ranges.⁶⁵ Variations correlate with U^{IV} coordination. The largest is observed for La-U₆, in which the majority of the U^{IV} sites are 9-coordinate (4 of 6), and the lowest is observed for Zn-U₇₀, in which the U sites are predominately 8-coordinate (56 of 70). Y-U₈₄, with an intermediate moment, contains almost half 8-coordinate U sites (48 of 84). All three compounds have large, negative paramagnetic Curie–Weiss temperatures, likely due to crystalline-electric field effects. The magnetic susceptibility of Mn-U₇₀ likewise exhibits Curie–Weiss behavior at high temperatures; however, no magnetic ordering is observed down to 2 K.

SUMMARY AND OUTLOOK

The TM^{II}-U^{IV} and Ln^{III}-U^{IV}-sulfate compounds described here are representative of a larger family that will be subsequently reported. This family features U₈₄, a “superatom” that organizes into superlattices with both heteroatom monomers and the U₆ unit of U₈₄. Superlattices assembled with small Ln^{III} include tetrahedral (interpenetrating), body-centered cubic and cubic-closest packed networks of U₈₄. The body-centered U₈₄ network-type mirrors U₆ networks with large Ln^{III}. U₈₄, comprised of 14 linked U₆, mirrors the arrangement of the U^{IV} monomers and sulfate bridges in U₆; thus, superlattices of U₈₄ can also be described as fractals with three generations. Because the closest U^{IV}-Ln or U^{IV}-TM connectivity is via a sulfate bridge in the reported compounds, there is no magnetic exchange or ordering. One future goal is to minimize or replace the sulfate in our syntheses and also promote isolation of U^V-containing analogues to access targeted magnetic synthons. The U₇₀ ring is a M^{IV} (M = Zr/Hf/An) cluster genre that has never been observed and also displays unique nonaqueous solubility and differing supramolecular assembly via TM^{II}-counterion linking. We will also access new superlattices of U₈₄ and U₇₀ from organic media, driving assembly from organic capping groups, as well as polyvalent counterion-linking.

EXPERIMENTAL SECTION

After discovering the initial crystalline forms, the syntheses with Ln were adjusted and optimized for yield and purity. In the optimized experiments, we combined mixtures of the oxides and chloride salts of the various lanthanides (see methods sections). Optimized syntheses are summarized here; details are provided in the Supporting Information along with procedures for single-crystal X-ray diffraction, magnetic measurements, SAXS, IR vibration spectroscopy, and TGA.

Caution! Although we are using depleted uranium (DU), it still possesses some radioactivity and is a toxic heavy metal, so precautions with suitable care and protection for handling each substance have been followed.

U(SO₄)₂, the reactant for all subsequent syntheses, is prepared from 5.0 g of uranyl(VI) acetate in 75 mL of anhydrous ethanol plus 25 mL of concentrated sulfuric acid. This solution is placed under UV light (390–400 nm, 15 W) for 24–48 h to obtain a green/purple U^{IV} sulfate powder. The solid is collected by vacuum filtration and washed with four 50 mL aliquots of ethanol (yield = 95.5%).

The Ln-U^{IV} (U₆ and U₈₄) compounds were all synthesized by similar methods, described generally here with details in the Supporting Information. U(SO₄)₂(100 mg, 0.23 mmol) is dissolved in 500 μL of 0.5 M H₂SO₄ in a 2 mL vial. The Ln is introduced as optimized mixtures of Ln₂O₃ plus LnCl₃. The vial is then placed in a sand bath and heated in an oven at 75 °C for 24 h. Crystallized products are then filtered out and washed with water followed by 0.5 M HCl to remove any soluble byproduct or starting material.

The TM-U^{IV} compounds (U₇₀) were synthesized as follows (details in Supporting Information). U(SO₄)₂ (100 mg, 0.23 mmol) is dissolved in 500 μL of H₂O in a 2 mL vial. TM^{II} (Zn, Mn) acetate was added, and the vial is then placed in a sand bath and heated in an oven at 75 °C for 24 h.

ASSOCIATED CONTENT

Supporting Information

The Supporting Information is available free of charge at <https://pubs.acs.org/doi/10.1021/jacs.0c03041>.

Detailed description of synthesis and other experimental methods, bulk characterization (IR, TGA), SAXS analyses, and crystallographic information (bond distances, BVS, detailed descriptions of disorder, and supplemental figures) ([PDF](#))

AUTHOR INFORMATION

Corresponding Author

May Nyman — Department of Chemistry, Oregon State

University, Corvallis, Oregon 97331, United States;

✉ orcid.org/0000-0002-1787-0518; Email: may.nyman@oregonstate.edu

Authors

Ian Colliard — Department of Chemistry, Oregon State University, Corvallis, Oregon 97331, United States

Gregory Morrison — Department of Chemistry and Biochemistry, University of South Carolina, Columbia, South Carolina 29208, United States; ✉ orcid.org/0000-0001-9674-9224

Hans-Conrad zur Loya — Department of Chemistry and Biochemistry, University of South Carolina, Columbia, South Carolina 29208, United States; ✉ orcid.org/0000-0001-7351-9098

Complete contact information is available at:

<https://pubs.acs.org/10.1021/jacs.0c03041>

Notes

The authors declare no competing financial interest.

ACKNOWLEDGMENTS

The synthesis and characterization of the reported compounds performed at OSU (M.N. and I.C.) is supported by the Department of Energy, National Nuclear Security Administration (NNSA) under Award DE-NA0003763. We acknowledge the Murdock Charitable Trust (Grant SR-2017297) for acquisition of the single-crystal X-ray diffractometer. The magnetic measurements performed at U of SC (G.M. and H.C.z.L.) was supported by the U.S. Department of Energy, Office of Science, Basic Energy Sciences, under Award DE-SC0016574 (Center for Hierarchical Waste Form Materials). I.C. thanks Dr. Nicolas Martin for advice and assistance with crystallography.

REFERENCES

- (1) Wang, L.; Liu, R.; Gu, J. L.; Song, B.; Wang, H.; Jiang, X.; Zhang, K. R.; Han, X.; Hao, X. Q.; Bai, S.; Wang, M.; Li, X. H.; Xu, B. Q.; Li, X. P. Self-Assembly of Supramolecular Fractals from Generation 1 to 5. *J. Am. Chem. Soc.* **2018**, *140* (43), 14087–14096.
- (2) Yang, H. B.; Northrop, B. H.; Zheng, Y. R.; Ghosh, K.; Stang, P. J. Facile Self-Assembly of Neutral Dendritic Metallocycles via Oxygeno-to-Platinum Coordination. *J. Org. Chem.* **2009**, *74* (18), 7067–7074.
- (3) Caminade, A. M.; Yan, D. Y.; Smith, D. K. Dendrimers and hyperbranched polymers. *Chem. Soc. Rev.* **2015**, *44* (12), 3870–3873.
- (4) Tomalia, D. A.; Naylor, A. M.; Goddard, W. A. Starburst Dendrimers - Molecular-Level Control of Size, Shape, Surface-Chemistry, Topology, and Flexibility from Atoms to Macroscopic Matter. *Angew. Chem., Int. Ed. Engl.* **1990**, *29* (2), 138–175.
- (5) Golub, E.; Subramanian, R. H.; Esselborn, J.; Alberstein, R. G.; Bailey, J. B.; Chiong, J. A.; Yan, X. D.; Booth, T.; Baker, T. S.; Tezcan, F. A. Constructing protein polyhedra via orthogonal chemical interactions. *Nature* **2020**, *578* (4851), 172–176.
- (6) Peng, Q.; Dong, Y. J.; Deng, Z. X.; Li, Y. D. Selective synthesis and characterization of CdSe nanorods and fractal nanocrystals. *Inorg. Chem.* **2002**, *41* (20), 5249–5254.
- (7) Shahzad, A.; Bhang, S. H.; Jung, E.; Kim, W. S.; Yu, T. Hierarchically structured 2D silver sheets with fractal network. *J. Materomics* **2018**, *4* (2), 121–128.
- (8) Rosseinsky, M. J. Fullerene Intercalation Chemistry. *J. Mater. Chem.* **1995**, *5* (10), 1497–1513.
- (9) Claridge, S. A.; Castleman, A. W.; Khanna, S. N.; Murray, C. B.; Sen, A.; Weiss, P. S. Cluster-Assembled Materials. *ACS Nano* **2009**, *3* (2), 244–255.
- (10) Liu, C.; Sun, Z. M. Recent advances in structural chemistry of Group 14 Zintl ions. *Coord. Chem. Rev.* **2019**, *382*, 32–56.
- (11) Mandal, S.; Reber, A. C.; Qian, M.; Liu, R.; Saavedra, H. M.; Sen, S.; Weiss, P. S.; Khanna, S. N.; Sen, A. Synthesis, structure and band gap energy of covalently linked cluster-assembled materials. *Dalton Transac* **2012**, *41* (40), 12365–12377.
- (12) Qian, M. C.; Reber, A. C.; Ugrinov, A.; Chaki, N. K.; Mandal, S.; Saavedra, H. M.; Khanna, S. N.; Sen, A.; Weiss, P. S. Cluster-Assembled Materials: Toward Nanomaterials with Precise Control over Properties. *ACS Nano* **2010**, *4* (1), 235–240.
- (13) Cavka, J. H.; Jakobsen, S.; Olsbye, U.; Guillou, N.; Lamberti, C.; Bordiga, S.; Lillerud, K. P. A new zirconium inorganic building brick forming metal organic frameworks with exceptional stability. *J. Am. Chem. Soc.* **2008**, *130* (42), 13850–13851.
- (14) Shepelev, Y. F.; Smolin, Y. I.; Ershov, A. S.; Rademaher, O.; Sheller, G. Determination of the Crystal-Structure of Sodiumtetramethylammonium Silicate $\text{Na}_7[\text{N}(\text{CH}_3)_4][\text{Si}_8\text{O}_{20}]\cdot 5\text{H}_2\text{O}$ at -120°C . *Kristallografiya* **1987**, *32* (6), 1399–1403.
- (15) Smolin, I. I.; Shepelev, I. F.; Ershov, A. S.; Hoebbel, D. Isolated Aluminosilicate Radical $[\text{Si}_4\text{Al}_4\text{O}_{12}(\text{OH})_8]$ in the Tetramethylammonium Aluminosilicate Crystal. *Dokl Akad Nauk SSSR* **1987**, *297* (6), 1377–1380.
- (16) Fedeyko, J. M.; Vlachos, D. G.; Lobo, R. F. Formation and structure of self-assembled silica nanoparticles in basic solutions of organic and inorganic cations. *Langmuir* **2005**, *21* (11), 5197–5206.
- (17) Mollick, S.; Fajal, S.; Mukherjee, S.; Ghosh, S. K. Stabilizing Metal-Organic Polyhedra (MOP): Issues and Strategies. *Chem. - Asian J.* **2019**, *14* (18), 3096–3108.
- (18) Muller, A.; Roy, S. En route from the mystery of molybdenum blue via related manipulatable building blocks to aspects of materials science. *Coord. Chem. Rev.* **2003**, *245* (1–2), 153–166.
- (19) Mitchell, S. G.; Boyd, T.; Miras, H. N.; Long, D. L.; Cronin, L. Extended polyoxometalate framework solids: two Mn(II)-linked $\{\text{P}_8\text{W}_{48}\}$ network arrays. *Inorg. Chem.* **2011**, *50* (1), 136–43.
- (20) Shmakova, A. A.; Volchek, V. V.; Yanshole, V.; Kompankov, N. B.; Martin, N. P.; Nyman, M.; Abramov, P. A.; Sokolov, M. N. Niobium uptake by a $[\text{P}_8\text{W}_{48}\text{O}_{184}]^{40-}$ macrocyclic polyanion. *New J. Chem.* **2019**, *43* (25), 9943–9952.
- (21) Martin, N. P.; Petrus, E.; Segado, M.; Arteaga, A.; Zakharov, L. N.; Bo, C.; Nyman, M. Strategic Capture of the $\{\text{Nb}_7\}$ Polyoxometalate. *Chem. - Eur. J.* **2019**, *25* (45), 10580–10584.
- (22) Zhu, Z. K.; Lin, Y. Y.; Yu, H.; Li, X. X.; Zheng, S. T. Inorganic-Organic Hybrid Polyoxoniobates: Polyoxoniobate Metal Complex Cage and Cage Framework. *Angew. Chem., Int. Ed.* **2019**, *58* (47), 16864–16868.
- (23) Zhang, J.; Lai, R. D.; Wu, Y. L.; Zhu, Z. K.; Sun, Y. Q.; Zeng, Q. X.; Li, X. X.; Zheng, S. T. High-dimensional Polyoxoniobates Constructed from Lanthanide-incorporated High-nuclear $\{[\text{Ln}(\text{H}_2\text{O})_4]_3 [\text{Nb}_{24}\text{O}_{69}(\text{H}_2\text{O})_{32}]\}$ Secondary Building Units. *Chem. - Asian J.* **2020**. DOI: [10.1002/asia.202000294](https://doi.org/10.1002/asia.202000294).
- (24) Qiu, J.; Ling, J.; Jouffret, L.; Thomas, R.; Szymanowski, J. E.; Burns, P. C. Water-soluble multi-cage super tetrahedral uranyl peroxide phosphate clusters. *Chem. Sci.* **2014**, *5* (1), 303–310.
- (25) Burns, P. C.; Nyman, M. Captivation with encapsulation: a dozen years of exploring uranyl peroxide capsules. *Dalton Trans* **2018**, *47* (17), 5916–5927.
- (26) Kalaji, A.; Soderholm, L. Aqueous Hafnium Sulfate Chemistry: Structures of Crystalline Precipitates. *Inorg. Chem.* **2014**, *53* (20), 11252–11260.
- (27) Knopke, K. E.; Vasiliu, M.; Dixon, D. A.; Soderholm, L. Thorium(IV)-Selenate Clusters Containing an Octanuclear Th(IV) Hydroxide/Oxide Core. *Inorg. Chem.* **2012**, *51* (7), 4239–4249.
- (28) Knopke, K. E.; Wilson, R. E.; Vasiliu, M.; Dixon, D. A.; Soderholm, L. Thorium(IV) Molecular Clusters with a Hexanuclear Th Core. *Inorg. Chem.* **2011**, *50* (19), 9696–9704.
- (29) Falaise, C.; Kozma, K.; Nyman, M. Thorium Oxo-Clusters as Building Blocks for Open Frameworks. *Chem. - Eur. J.* **2018**, *24* (53), 14226–14232.
- (30) Yue, Z.; Guo, X.; Feng, M. L.; Lin, Y. J.; Ju, Y.; Lin, X.; Zhang, Z. H.; Guo, X.; Lin, J.; Huang, Y. Y.; Wang, J. Q. Unexpected Roles of Alkali-Metal Cations in the Assembly of Low-Valent Uranium Sulfate Molecular Complexes. *Inorg. Chem.* **2020**, *59* (4), 2348–2357.
- (31) Takao, S.; Takao, K.; Kraus, W.; Emmerling, F.; Scheinost, A. C.; Bernhard, G.; Hennig, C. First Hexanuclear U^{IV} and Th^{IV} Formate Complexes - Structure and Stability Range in Aqueous Solution. *Eur. J. Inorg. Chem.* **2009**, *32*, 4771–4775.
- (32) Lin, J.; Jin, G. B.; Soderholm, L. $\text{Th}_3[\text{Th}_6(\text{OH})_4\text{O}_4(\text{H}_2\text{O})_6]\cdot (\text{SO}_4)_{12}(\text{H}_2\text{O})_{13}$: A Self-Assembled Microporous Open-Framework Thorium Sulfate. *Inorg. Chem.* **2016**, *55* (20), 10098–10101.
- (33) Falaise, C.; Charles, J. S.; Volkinger, C.; Loiseau, T. Thorium Terephthalates Coordination Polymers Synthesized in Solvothermal DMF/H₂O System. *Inorg. Chem.* **2015**, *54* (5), 2235–2242.
- (34) Loiseau, T.; Mihalcea, I.; Henry, N.; Volkinger, C. The crystal chemistry of uranium carboxylates. *Coord. Chem. Rev.* **2014**, *266*, 69–109.
- (35) Ejegbabwo, O. A.; Martin, C. R.; Olorunfemi, O. A.; Leith, G. A.; Ly, R. T.; Rice, A. M.; Dolgopolova, E. A.; Smith, M. D.; Karakalos, S. G.; Birkner, N.; Powell, B. A.; Pandey, S.; Koch, R. J.; Misture, S. T.; Loyer, H. C. Z.; Phillipot, S. R.; Brinkman, K. S.; Shustova, N. B. Thermodynamics and Electronic Properties of Heterometallic Multinuclear Actinide-Containing Metal-Organic

- Frameworks with “Structural Memory. *J. Am. Chem. Soc.* **2019**, *141* (29), 11628–11640.
- (36) Martin, N. P.; Marz, J.; Feuchter, H.; Duval, S.; Roussel, P.; Henry, N.; Ikeda-Ohno, A.; Loiseau, T.; Volkrieger, C. Synthesis and structural characterization of the first neptunium based metal-organic frameworks incorporating $\{Np_6O_8\}$ hexanuclear clusters. *Chem. Commun.* **2018**, *54* (51), 6979–6982.
- (37) Biswas, B.; Mougel, V.; Pecaut, J.; Mazzanti, M. Base-Driven Assembly of Large Uranium Oxo/Hydroxo Clusters. *Angew. Chem., Int. Ed.* **2011**, *50* (25), 5744–5747.
- (38) Dufaye, M.; Martin, N. P.; Duval, S.; Volkrieger, C.; Ikeda-Ohno, A.; Loiseau, T. Time-controlled synthesis of the 3D coordination polymer $U(1,2,3-Hbtc)_2$ followed by the formation of molecular poly-oxo cluster $\{U_{14}\}$ containing hemimellitate uranium(IV). *RSC Adv.* **2019**, *9* (40), 22795–22804.
- (39) Falaise, C.; Volkrieger, C.; Vigier, J. F.; Beaureain, A.; Roussel, P.; Rabu, P.; Loiseau, T. Isolation of the Large $\{\text{Actinide}\}_{38}$ Poly-oxo Cluster with Uranium. *J. Am. Chem. Soc.* **2013**, *135* (42), 15678–15681.
- (40) Martin, N. P.; Volkrieger, C.; Henry, N.; Trivelli, X.; Stoclet, G.; Ikeda-Ohno, A.; Loiseau, T. Formation of a new type of uranium(IV) poly-oxo cluster $\{U_{38}\}$ based on a controlled release of water via esterification reaction. *Chem. Sci.* **2018**, *9* (22), 5021–5032.
- (41) Sigmon, G. E.; Hixon, A. E. Extension of the Plutonium Oxide Nanocluster Family to Include $\{Pu_{16}\}$ and $\{Pu_{22}\}$. *Chem. - Eur. J.* **2019**, *25* (10), 2463–2466.
- (42) Soderholm, L.; Almond, P. M.; Skanthakumar, S.; Wilson, R. E.; Burns, P. C. The structure of the plutonium oxide nanocluster $[Pu_{38}O_{56}Cl_{54}(H_2O)_8]^{14-}$. *Angew. Chem., Int. Ed.* **2008**, *47* (2), 298–302.
- (43) Martin, N. P.; Volkrieger, C.; Roussel, P.; Marz, J.; Hennig, C.; Loiseau, T.; Ikeda-Ohno, A. $\{Np_{38}\}$ clusters: the missing link in the largest poly-oxo cluster series of tetravalent actinides. *Chem. Commun.* **2018**, *54* (72), 10060–10063.
- (44) Novikov, A. P.; Kalmykov, S. N.; Utsunomiya, S.; Ewing, R. C.; Horreard, F.; Merkulov, A.; Clark, S. B.; Tkachev, V. V.; Myasoedov, B. F. Colloid transport of plutonium in the far-field of the Mayak Production Association, Russia. *Science* **2006**, *314* (5799), 638–641.
- (45) Hennig, C.; Kraus, W.; Emmerling, F.; Ikeda, A.; Scheinost, A. C. Coordination of a uranium(IV) sulfate monomer in an aqueous solution and in the solid state. *Inorg. Chem.* **2008**, *47* (5), 1634–8.
- (46) Schnaars, D. D.; Wilson, R. E. Uranium(IV) sulfates: investigating structural periodicity in the tetravalent actinides. *Inorg. Chem.* **2012**, *51* (17), 9481–90.
- (47) Suzuki, Y.; Kelly, S. D.; Kemner, K. M.; Banfield, J. F. Radionuclide contamination - Nanometre-size products of uranium bioreduction. *Nature* **2002**, *419* (6903), 134–134.
- (48) Sommers, J. A.; Hutchison, D. C.; Martin, N. P.; Kozma, K.; Keszler, D. A.; Nyman, M. Peroxide-Promoted Disassembly Reassembly of Zr-Polyoxocations. *J. Am. Chem. Soc.* **2019**, *141* (42), 16894–16902.
- (49) Vinslava, A.; Tasiopoulos, A. J.; Wernsdorfer, W.; Abboud, K. A.; Christou, G. Molecules at the Quantum-Classical Nanoparticle Interface: Giant Mn_{70} Single-Molecule Magnets of similar to 4 nm Diameter. *Inorg. Chem.* **2016**, *55* (7), 3419–3430.
- (50) Xu, F.; Miras, H. N.; Scullion, R. A.; Long, D. L.; Thiel, J.; Cronin, L. Correlating the magic numbers of inorganic nanomolecular assemblies with a $\{Pd_{84}\}$ molecular ring Rosetta Stone. *Proc. Natl. Acad. Sci. U. S. A.* **2012**, *109* (29), 11609–11612.
- (51) Knope, K. E.; Vanagas, N. A.; Higgins, R. F.; Wacker, J. N.; Romar, D.; Asuigui, C.; Warzecha, E.; Kozmor, S. A.; Stoll, S. L.; Schelter, E. J.; Bertke, J. A., Mononuclear to Polynuclear U(IV) Structural Units: Effects of Reaction Conditions on U-Furoate Phase Formation. *Chem. - Eur. J.* **2020**. DOI: 10.1002/chem.201905759.
- (52) Misra, A.; Kozma, K.; Streb, C.; Nyman, M. Beyond Charge Balance: Counter-Cations in Polyoxometalate Chemistry. *Angew. Chem., Int. Ed.* **2020**, *132* (2), 596–612.
- (53) Knope, K. E.; Soderholm, L. Solution and Solid-State Structural Chemistry of Actinide Hydrates and Their Hydrolysis and Condensation Products. *Chem. Rev.* **2013**, *113* (2), 944–994.
- (54) Perkins, C. K.; Eitrheim, E. S.; Fulton, B. L.; Fullmer, L. B.; Colla, C. A.; Park, D. H.; Oliveri, A. F.; Hutchison, J. E.; Nyman, M.; Casey, W. H.; Forbes, T. Z.; Johnson, D. W.; Keszler, D. A. Synthesis of an Aluminum Hydroxide Octamer through a Simple Dissolution Method. *Angew. Chem., Int. Ed.* **2017**, *56* (34), 10161–10164.
- (55) Lundgren, G. The Crystal Structure of $U_6O_4(OH)_4(SO_4)_6$. *Ark. Kemi* **1953**, *5*, 349–363.
- (56) Loble, M. W.; Keith, J. M.; Altman, A. B.; Stieber, S. C. E.; Batista, E. R.; Boland, K. S.; Conradson, S. D.; Clark, D. L.; Lezama Pacheco, J.; Kozmor, S. A.; Martin, R. L.; Minasian, S. G.; Olson, A. C.; Scott, B. L.; Shuh, D. K.; Tyliszczak, T.; Wilkerson, M. P.; Zehnder, R. A. Covalency in Lanthanides. An X-ray Absorption Spectroscopy and Density Functional Theory Study of $LnCl_6^x$ ($x = 3, 2$). *J. Am. Chem. Soc.* **2015**, *137* (7), 2506–2523.
- (57) Frank, P.; Szilagyi, R. K.; Gramlich, V.; Hsu, H. F.; Hedman, B.; Hodgson, K. O. Spin-Polarization-Induced Preedge Transitions in the Sulfur K-Edge XAS Spectra of Open-Shell Transition-Metal Sulfates: Spectroscopic Validation of sigma-Bond Electron Transfer. *Inorg. Chem.* **2017**, *56* (3), 1080–1093.
- (58) Shevchenko, E. V.; Talapin, D. V.; Murray, C. B.; O’Brien, S. Structural characterization of self-assembled multifunctional binary nanoparticle superlattices. *J. Am. Chem. Soc.* **2006**, *128* (11), 3620–3637.
- (59) Chen, Z.; O’Brien, S. Structure direction of II-VI semiconductor quantum dot binary nanoparticle superlattices by tuning radius ratio. *ACS Nano* **2008**, *2* (6), 1219–1229.
- (60) Sessoli, R.; Powell, A. K. Strategies towards single molecule magnets based on lanthanide ions. *Coord. Chem. Rev.* **2009**, *293* (19–20), 2328–2341.
- (61) Vanagas, N. A.; Wacker, J. N.; Rom, C. L.; Glass, E. N.; Colliard, I.; Qiao, Y. S.; Bertke, J. A.; Van Keuren, E.; Schelter, E. J.; Nyman, M.; Knope, K. E. Solution and Solid State Structural Chemistry of Th(IV) and U(IV) 4-Hydroxybenzoates. *Inorg. Chem.* **2018**, *57* (12), 7259–7269.
- (62) Usman, M.; Morrison, G.; Klepov, V. V.; Smith, M. D.; zur Loya, H. C. Flux crystal growth, structure, magnetic and optical properties of a family of alkali uranium(IV) phosphates. *J. Solid State Chem.* **2019**, *270*, 19–26.
- (63) Morrison, G.; Ramanantoanina, H.; Urland, W.; Smith, M. D.; zur Loya, H.-C. Flux Synthesis, Structure, Properties, and Theoretical Magnetic Study of Uranium(IV)-Containing $A_2USi_6O_{15}$ ($A = K, Rb$) with an Intriguing Green-to-Purple, Crystal-to-Crystal Structural Transition in the K Analogue. *Inorg. Chem.* **2015**, *54* (11), 5504–5511.
- (64) Klepov, V. V.; Pace, K. A.; Calder, S.; Felder, J. B.; zur Loya, H. C. 3d-Metal Induced Magnetic Ordering on U(IV) Atoms as a Route toward U(IV) Magnetic Materials. *J. Am. Chem. Soc.* **2019**, *141* (9), 3838–3842.
- (65) Kindra, D. R.; Evans, W. J. Magnetic Susceptibility of Uranium Complexes. *Chem. Rev.* **2014**, *114* (18), 8865–8882.